# CONSTANT PHASE ELEMENT (CPE) MODELING AND ANALYSIS OF MULTI-MATERIAL, MICRO-BULLET SHAPED, HIGH-THROUGHPUT 3D MICROELECTRODES FOR *IN-VITRO* ELECTROPHYSIOLOGICAL APPLICATIONS

*Jorge Manrique Castro, and Swaminathan Rajaraman*
University of Central Florida, Orlando, Florida, USA

## ABSTRACT

***This paper reports for the first time*, modeling, and analysis of Electrochemical Impedance Spectroscopy (EIS) from micro-bullet shaped 3D microelectrodes fabricated in high-throughput array (HT) formats with three different materials [Gold, Biocompatible-Silver Paste and Microelectronic-Silver Paste] in electrode-electrolyte interface. The modeling was based on the Randles' Electrochemical Equivalent Circuit (EEC) with a *Constant Phase Element (CPE) driving element* and impedance data collected from HT-3D Microelectrode Arrays (MEAs) was fitted. *CPE was determined as an excellent adaptative element* for electrical representation in MEA models due to low error per element during fitting process into EEC, and *exceptional matching observed between modeling and experiments* opening new avenues into the understanding of electrochemical interaction of 3D microelectrodes.**

## KEYWORDS

3D Microelectrode Arrays (3D MEAs), Modeling, Constant Phase Element (CPE), High-Throughput, Electrochemical Impedance Spectroscopy (EIS).

## INTRODUCTION

Electrogenic cell studies are critical for understanding the response of a variety of biological entities under the influence of physicochemical reactions caused by the interaction with their surroundings. This interaction might be caused by drugs, diseases, or environmental conditions **[1]**.

*In-vitro* studies provide an excellent approach to researchers and laboratories in order to quantify these interactions with functional readouts, and devices equipped with microelectrodes are widely used as means for obtaining electrical signatures from the cultured cells and cellular networks **[2]**. 3D MEAs are being explored as an alternative to the traditional 2D MEAs in *in-vitro* studies in an attempt to improve the spatial and temporal resolution with access provided deeper into the tissue architecture from 3D microelectrode configuration **[3]**. 3D features can be formed using a diversity of materials, each having its inherent physical and chemical properties in addition to a variety of processing methods. Structure of microelectrodes employed into the MEAs is paramount to getting reliable electrical signals (i.e., recording) or providing a charge to the cell/network (i.e., stimulation) **[4]**.

Electrode modeling techniques have been widely investigated by using EECs that provide a fitted response to redox reactions near the electrode surface. Several techniques such as EIS can be applied to record electrical information from MEAs. While 2D MEAs have been modeled using Finite Element Modeling (FEM) **[5]** and other studies have expanded to having theoretical implications for 3D microelectrodes including Method of Images (MoI) **[6]**, there still remains a gap in modeling of 3D microelectrodes due to the non-homogeneity of 3D structures.

3D electrode geometry is key to EIS data which is controlled by various materials and microfabrication processes **[7, 8]**. Electrochemical cells are modeled typically using Randles' EEC **[7]**, widely used in biomedical applications with kinetic and diffusion elements involving electrodes/electrolyte interface for homogeneous and non-homogeneous systems. In order to get the maximum microelectrode selectivity for recording and stimulation in biological settings, a balance between size and impedance is paramount and needs to be considered **[8]**.

Theoretical elements such as Warburg provide a representation of the impedance related to Faradaic processes caused by the diffusion of species. Due to the nature of the microelectrode under analysis, this response might show some tendencies to behave capacitively in the case of a reflective boundary or as a short in the case of transmissive boundary **[9]**. This variability opens up opportunities in terms of adding new elements to electrode modeling, and the CPE presented in this work fits nicely to diffusion

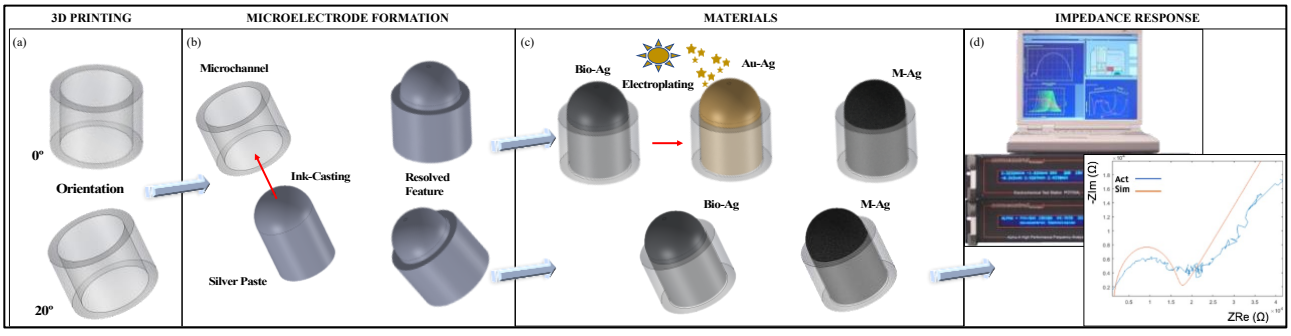


***Figure 1:*** *Schematic process for microelectrodes fabrication and impedance analysis in a sequential fashion. (a): 3D microchannel 3D printed at 0° and 20° with respect to the resin plane using micro-stereolithography. (b): 3D Microelectrode fabrication using an Ink-Casting technique and resolved features for both printing angles after silver paste curing. (c): Materials used to characterize 3D microelectrodes, for 0°, Au-Ag and M-Ag were studied. Au-Ag was fabricated using electroplating atop the Ag paste. On the other hand, for 20°, Bio-Ag and M-Ag were studied. (d): Electrochemical impedance spectroscopy testing showcasing Nyquist and Bode plots responses that were modeled.*

978-1-940470-04-7/HH2022/$25©2022TRF
DOI 10.31438/trf.hh2022.101

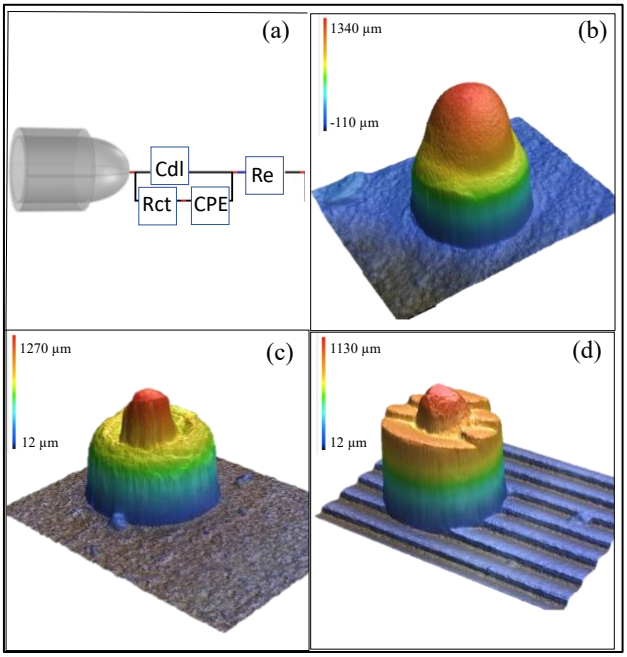


***Figure 2:*** *(a): Randles' EEC model for impedance modeling with Constant Phase Element (CPE [Q, α]). (b-d): Laser confocal microelectrodes characterization for the 3D microelectrodes: (b): Au-Ag at 0º, (c): Bio-Ag at 0º and (d): M-Ag at 20º.*

effects obtained from real measurements due to its versatile theoretical definition.

3D microelectrodes present unique challenges to modeling since 3D electrode geometry is key to EIS data and its response is electrode surface dependent, which is provided by different materials and microfabrication processes. ***CPE is a potential element that is used to fit data for the interpretation of various kinetic and diffusion processes [10] involved in the electrochemistry of in-vitro applications***.

## MATERIALS AND METHODS

The detailed microfabrication approach used for these HT-3D MEAs is described in our recently published IEEE JMEMS article **[11]**. Only a brief description of the methods used in this work are detailed below. For more information, the reader is referred to the JMEMS paper. Computer-aided design (CAD) software was employed for the 3D printed microstructures that served as support structure for the microelectrodes. After post processing the 3D printed structures, the microstructures were filled with three different materials and their impedance performance was measured utilizing EIS with a vector analyzer tool. Physical characteristics of the 3D microelectrodes were obtained using 3D surface optical profilometry and Scanning Electron Microscopy (SEM) techniques. Lastly, modeling was performed comparing sets of actual impedance data vs. fitted impedance data, after parameters were extracted from the frequency response of the impedance and phase spectrum.

### Microelectrode Design

Multi-well bioplates were designed using CAD software (Solidworks, Dassault Systèmes) with each well containing a variety of microelectrodes. In total, 168 microchannels (7 per well) serving as microelectrode main structure were designed having dimensions of 800 µm height, 1000 µm OD and 800 µm ID. The design included

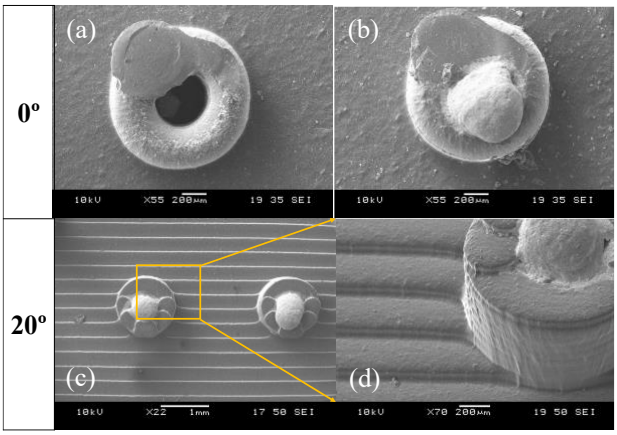


***Figure 3:*** *SEM images of silver-ink cast 3D microelectrodes at 0º and 20º tilt printing angles. Microchannel unfilled in (a) and filled in (b). (c): Top view of MEA. (d): Magnified view of the electrode structure/electrode surface at 180º rotation and 25º tilt in SEM.*

the traces from the back side of the bioplates serving as interface for further electrical characterization with dimensions of 400 µm width by 400 µm depth. The length of these traces was varied depending on the 3D microelectrode and well location.

### Microchannel 3D Printing

Microfabrication of electrode microchannels was carried out by using 3D printing (Form 3, Formlabs), based on the working principle of micro-stereolithography (µSLA). Optimization of processes led to our 6/12-well HT-3D MEAs **[12]**, being scaled to the microfabrication of 168 micro-bullet shaped electrodes in a 24-well HT-3D MEA format **[13]**, eliminating short circuits and traces openings in metallization, and reducing mechanical abrasion steps needed to improve surface quality. The microchannels were printed at 0º and 20º tilt angle with opposite orientation with respect to the base plane.

### Metallization

Metallization process was performed using an in-house ink-casting technique and three combinations of materials were selected for this research. Ink-casting with Au coated (Gold Plating Solution TSG-250, Transene Company) biocompatible silver paste [Au-Ag], biocompatible silver paste [Bio-Ag] (EP3HTSMED, Masterbond), and microelectronic silver epoxy [M-Ag] (Prima-Solder EG8050, AI Technology) materials were used to ***define 3D microelectrodes at 0º and 20º 3D printing angle*** (**Figure 1**). Au-Ag material was a composite material, whose surface was modified by Au electroplating, using a 50% AC cycle square pulse of amplitude 1 A/cm$^2$ for 30 s run in a customized LabView executable program. Sulfite gold plating solution (TSG-250, Transene Company) was employed for this electrochemical process.

### Optical Characterization

Mechanical structure of the optimized version of the 24-well HT-3D MEAs was analyzed using laser confocal 3D microscopy (VK-X3000, Keyence) and scanning electron microscopy (SEM, JSM-6480, JEOL) to identify microelectrodes/microchannels integrity and surface homogeneity in the metalized electrodes.

### Electrical Characterization

Electrochemical impedance spectroscopy was performed using

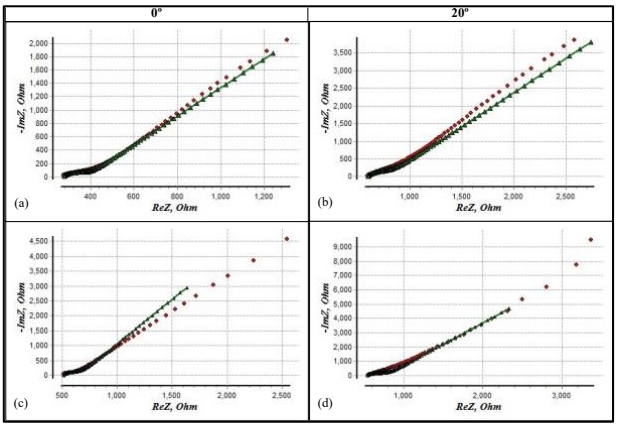


***Figure 4:*** *Nyquist plots for experimental (EIS data) and theoretical (EEC Fitted Model) results implementing EISSA software approach with CPE as driving element of the electrochemical cell. Plots for Au-Ag and Bio-Ag paste-based microelectrodes are shown in (a) and (b) respectively. Plots for M-Ag epoxy-based microelectrodes are depicted in (c) and (d). EISSA experimental data is plotted in red, fitted data in green. Columns provide information about the printing angle used in micro-stereolithography.*

a Vector Network Analyzer (Bode 100, Omicron Lab) utilizing phosphate buffer solution (PBS) as electrolyte and Pt/Ti wire as counter electrode. Electrical modeling involved theoretical fitting of data from EIS and post-processing in the electrophysiologically useful spectrum range (1Hz-10kHz) **[8]** including Nyquist/Bode plots at electrophysiologically-relevant 1kHz **[14]**.

### Modeling

Post-processing was performed using ***EIS Spectrum Analyzer (EISSA) software*** **[15]**. Experimental data was compared to Randles' EEC model with the extraction of resistive, capacitive and diffusion parameter (represented by CPE) to obtain the best fitting model based on these electrical parameters.

***Table I:*** *Extracted parameters from the fitted models for the 0° and 20° printing orientation 3D microelectrodes*

| Microelectrode 3D printed version | $R_e$ (Ω) | $R_{ct}$ (Ω) | $C_{dl}$ (nF) | CPE [Q] ($\mu\Omega^{-1}.s^{\alpha}$) | CPE [α] |
|---|---|---|---|---|---|
| **Biocompatible Gold/Silver Paste (Au-Ag)** | | | | | |
| 0°[a] | 278 | 118 | 2079 | 128 | 0.72 |
| Error (%) | 1.8 | 7.4 | 8.7 | 4.0 | 1.4 |
| 20°[b] | 598 | 239 | 1733 | 63.8 | 0.69 |
| Error (%) | 1.4 | 7.5 | 9.9 | 3.0 | 1.5 |
| **Microelectronic Silver Epoxy (M-Ag)** | | | | | |
| 0° | 516 | 200 | 4500 | 70.3 | 0.78 |
| Error (%) | 5.6 | 9.9 | 9.9 | 4.5 | 2.1 |
| 20°[b] | 543 | 297 | 2020 | 45 | 0.79 |
| Error (%) | 1.3 | 3.8 | 7.4 | 5.5 | 3.3 |

[a] *Au electroplated.* [b] *Bottom-side 3D printed orientation.*

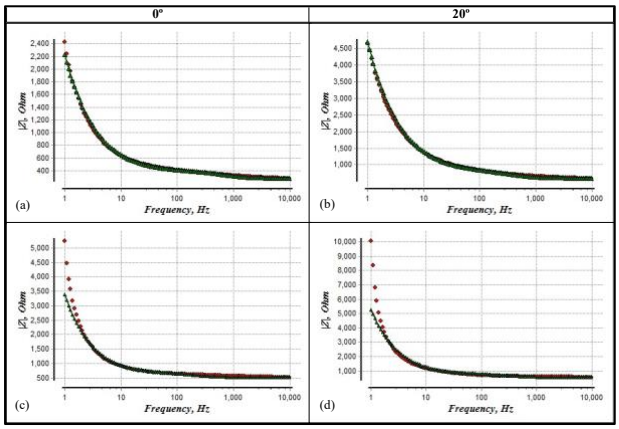


***Figure 5:*** *Bode magnitude plots for experimental (EIS data) and theoretical (EEC Fitted Model) results implementing EISSA software approach with CPE as driving element of the electrochemical cell. Plots for Au-Ag and Bio-Ag paste-based microelectrodes are shown in (a) and (b) respectively. Plots for M-Ag epoxy-based microelectrodes are depicted in (c) and (d). EISSA experimental data is plotted in red, fitted data in green. Columns provide information about the printing angle used in micro-stereolithography.*

## RESULTS AND DISCUSSIONS

Modified EEC Randles' model along 3D microelectrode profiles for Au-Ag, Bio-Ag and M-Ag materials are depicted in **Figure 2** and SEM images in **Figure 3**, ***showcasing the micro-bullet shape*** emanating from the microchannel structure, ideal for recording/ stimulation cell studies **[16]**. EIS comparison between the experimental and modeling data using EISSA software are depicted in **Figures 4 and 5**. Real impedance of ***317 Ω was obtained at 1kHz frequency*** for the ***Au-Ag material*** (0° print angle) which is ***exceptionally low for biomedical signaling*** in the electrophysiological range (100Hz to 3kHz) **[5]**. Modeling optimization with CPE found it as suitable diffusion element with ***α ranging from 0.69 to 0.79*** showing a diffusion-capacitive mixed behavior, and ***Q ranging from 45 to 128 $\mu\Omega^{-1}.s^{\alpha}$*** similar to literature reports when used as interface capacitance element **[17]**.

Interesting differences (8% at 0° printing and 13% at 20° printing) for α value in the Au-Ag and Bio-Ag vs M-Ag microelectrodes were found ***clearly depicting the effect of microfabrication and materials on electrode homogeneity*** (surface roughness and porosity). For Au-Ag electrodes, variability in coating thickness due to the electroplated Au is an additional contributor, acting as a surface structure modifier. ***Au-Ag and Bio-Ag microelectrodes presented a more diffusional impedance behavior than M-Ag due to α approaching the ideal value of 0.5*** **[18]**.

Values of the extracted parameters for micro-bullet microelectrodes are summarized in **Table I**. Errors after fitting of $R_e$, $R_{ct}$, $C_{dl}$, Q and α were all estimated to be ***less than 10 %***. These results prove that impedance response and diffusional effects can be modeled for 3D microelectrodes using different materials with high degree of accuracy showing advance in the field for features and functional structures beyond the traditional 2D microelectrodes.

## CONCLUSIONS

This investigation demonstrates that materials properties in the conformation of electrode surface for 3D features play an important role in the recording of electrogenic cells for biomedical studies due

to its particular signature when different electrochemical interactions are present.

Electrode modeling driven by CPE elements in the faradaic and non-faradaic processes provided an excellent fitting approach due to its theoretical versatility, where adjustable parameters can lead to a finer matching between the impedance and phase responses to the actual data from microfabricated electrodes.

## ACKNOWLEDGEMENTS

This work was supported by the University of Central Florida Research Foundation (UCFRF) funding using the GAP program. The authors would additionally like to acknowledge the Nanoscience Technology Center (NSTC) and UCF Graduate Studies for providing funding to present this research on the Hilton Head MEMS 2022 Workshop. Also, special thanks to Transducer Research Foundation (TRF) for the travel grant provided to JMC as presenting author.

## REFERENCES

[1] J. S. Choi, H. J. Lee, S. Rajaraman, and D.-H. Kim, "Recent advances in three-dimensional microelectrode array technologies for in vitro and in vivo cardiac and neuronal interfaces," *Biosensors and Bioelectronics,* vol. 171, p. 112687, 2021/01/01/ 2021, doi: https://doi.org/10.1016/j.bios.2020.112687.

[2] C. M. Didier, A. Kundu, J. M. Castro, C. Hart, and S. Rajaraman, "Compact Micro-Stereolithographic (μSLA) Printed, 3D Microelectrode Arrays (3D MEAS) with Monolithically Defined Positive and Negative Relief Features For in Vitro Cardiac Beat Sensing," in *2022 IEEE 35th International Conference on Micro Electro Mechanical Systems Conference (MEMS)*, 9-13 Jan. 2022 2022, pp. 325-328, doi: 10.1109/MEMS51670.2022.9699662.

[3] F. Santoro *et al.*, "Interfacing Electrogenic Cells with 3D Nanoelectrodes: Position, Shape, and Size Matter," *ACS Nano,* vol. 8, no. 7, pp. 6713-6723, 2014/07/22 2014, doi: 10.1021/nn500393p.

[4] K. D. Wise, A. M. Sodagar, Y. Yao, M. N. Gulari, G. E. Perlin, and K. Najafi, "Microelectrodes, Microelectronics, and Implantable Neural Microsystems," *Proceedings of the IEEE,* vol. 96, no. 7, pp. 1184-1202, 2008, doi: 10.1109/JPROC.2008.922564.

[5] C. Moulin *et al.*, "A New 3-D Finite-Element Model Based on Thin-Film Approximation for Microelectrode Array Recording of Extracellular Action Potential," *IEEE Transactions on Biomedical Engineering,* vol. 55, no. 2, pp. 683-692, 2008, doi: 10.1109/TBME.2007.903522.

[6] T. V. Ness *et al.*, "Modelling and Analysis of Electrical Potentials Recorded in Microelectrode Arrays (MEAs)," *Neuroinformatics,* vol. 13, no. 4, pp. 403-426, 2015/10/01 2015, doi: 10.1007/s12021-015-9265-6.

[7] Z. Wang, A. Murphy, A. O'Riordan, and I. O'Connell, "Equivalent Impedance Models for Electrochemical Nanosensor-Based Integrated System Design," *Sensors,* vol. 21, no. 9, 2021, doi: 10.3390/s21093259.

[8] G. Kovacs, "Introduction to the theory, design, and modeling of thin-film microelectrodes for neural interfaces," *Enabling technologies for cultured neural networks,* 1994.

[9] "Impedance Representation of Bulk-Material and Electrode Processes," in *Impedance Spectroscopy*, 2012, pp. 59-96.

[10] J.-B. Jorcin, M. E. Orazem, N. Pébère, and B. Tribollet, "CPE analysis by local electrochemical impedance spectroscopy," *Electrochimica Acta,* vol. 51, no. 8, pp. 1473-1479, 2006/01/20/ 2006, doi: https://doi.org/10.1016/j.electacta.2005.02.128.

[11] J. M. Castro and S. Rajaraman, "Experimental and Modeling Based Investigations of Process Parameters on a Novel, 3D Printed and Self-Insulated 24-Well, High-Throughput 3D Microelectrode Array Device for Biological Applications," *Journal of Microelectromechanical Systems,* pp. 1-14, 2022, doi: 10.1109/JMEMS.2022.3160663.

[12] A. Kundu, A. Rozman, and S. Rajaraman, "Development of a 3D Printed, Self-Insulated, High-Throughput 3D Microelectrode Array (HT-3DMEA)," *Journal of Microelectromechanical Systems,* vol. 29, no. 5, pp. 1091-1093, 2020, doi: 10.1109/JMEMS.2020.3003644.

[13] J. M. Castro, A. Kundu, A. Rozman, and S. Rajaraman, "Investigation of the Effect of Printing Angle and Device Orientation on Micro-Stereolithographically Printed, and Self-insulated, 24-well, High-Throughput 3D Microelectrode Arrays," in *2021 IEEE Sensors*, 31 Oct.-3 Nov. 2021 2021, pp. 1-4, doi: 10.1109/SENSORS47087.2021.9639637.

[14] Y. H. Kim, A. Y. Kim, G. H. Kim, Y. H. Han, M.-A. Chung, and S.-D. Jung, "Electrochemical and in vitro neuronal recording characteristics of multi-electrode arrays surface-modified with electro-co-deposited gold-platinum nanoparticles," *Biomedical Microdevices,* vol. 18, no. 1, p. 14, 2016/02/01 2016, doi: 10.1007/s10544-016-0044-4.

[15] A. Bondarenko and G. Ragoisha, "Inverse Problem In Potentiodynamic Electrochemical Impedance," in *Progress in Chemometrics Research*, A. L. Pomerantsev Ed. New York: Nova Science Publishers, 2005, pp. 89-102.

[16] C. M. Didier, A. Kundu, D. DeRoo, and S. Rajaraman, "Development of in vitro 2D and 3D microelectrode arrays and their role in advancing biomedical research," *Journal of Micromechanics and Microengineering,* vol. 30, no. 10, p. 103001, 2020/07/21 2020, doi: 10.1088/1361-6439/ab8e91.

[17] W. Franks, I. Schenker, P. Schmutz, and A. Hierlemann, "Impedance characterization and modeling of electrodes for biomedical applications," *IEEE Transactions on Biomedical Engineering,* vol. 52, no. 7, pp. 1295-1302, 2005, doi: 10.1109/TBME.2005.847523.

[18] S. Wang, J. Zhang, O. Gharbi, V. Vivier, M. Gao, and M. E. Orazem, "Electrochemical impedance spectroscopy," *Nature Reviews Methods Primers,* vol. 1, no. 1, p. 41, 2021/06/10 2021, doi: 10.1038/s43586-021-00039-w.

## CONTACT

*Swaminathan Rajaraman, tel: +1-407-823-4339; swaminathan.rajaraman@ucf.edu